Fusion of telescopic and Doppler radar data

Mirko Navara[1], Martin Matoušek[1], Ondřej Drbohlav[2]

[1] *Czech Technical University in Prague, Czech Institute of Informatics, Robotics, and Cybernetics, Department of Robotics and Machine Perception, Czech Republic*

[2] *Czech Technical University in Prague, Faculty of Electrical Engineering, Department of Cybernetics, Center for Machine Perception, Czech Republic*

{navara,xmatousm,drbohlav}@cmp.felk.cvut.cz

ABSTRACT

The most usual ways of observation of satellites and space debris and measurement of their orbits are

- telescopic images,
- radar reflections,
- laser measurements.

We use two of these three modalities, we combine telescopic images with response of Doppler radars. We use single images from a terrestrial telescope. Our radar is passive, we receive the signal of a distant terrestrial transmitter. The receiver has a *non-directional antenna* and only *Doppler shift* is employed to gain information about an object's movement. Due to sensitivity limitations, our approach is applicable to large objects (RCS $\geq 5\,\mathrm{m}^2$) at distances ≤ 2000 km. Our method requires simultaneous detections by a telescope and a radar during the same fly-over, not necessarily at exactly the same time.

I. WHAT CAN AND WHAT CANNOT BE DETERMINED FROM TELESCOPIC IMAGES

We have data from the telescope at Ondřejov observatory (N 49.9091°, E 14.791966°, 528 m altitude) of the Astronomical Institute of the Czech Academy of Sciences. The telescope has a mirror with diameter 60 cm and field of view 20′ and is equipped with a 1054×1027 CCD camera, thus having resolution 1.177"/pixel. The images are taken with or without sidereal tracking; this influences the methods and sensitivity of detection, but not much the principal information obtained.

Our observation (a single image or a sequence of images taken during a single fly-over) allows us to determine up to 4 orbital parameters. This is sufficient for the estimation of a circular orbit. This is true under optimal conditions when the object is seen as a short line segment (*streak*) with both endpoints inside the image, so that they correspond to the beginning and end of the exposure time.

Near GEO objects with almost circular orbits usually allow us to estimate all important orbital parameters. These violate the assumptions only with a low probability—if the object enters/leaves the FOV during the exposure or if it is not visible all the time due to reflections, background stars, etc. There is also another uncertainty—we cannot distinguish the beginning of the streak from its end, thus we have two possibilities which cannot be recognized from the image alone.

LEO objects usually pass through the whole FOV during the exposure, thus we know only a line in the image which contains the projected trajectory. Due to an imprecise timing, we even *do not know the plane* in space containing the orbit. Knowing a line in a 2D image, we can reduce the number of degrees of freedom by 2. One possible solution is to use a camera with a wide FOV, so that the endpoints are inside the image. However, this leads to a very imprecise localisation.

For *HEO objects*, the endpoints of a streak may or may not be visible in the image, but the assumption of circular orbits is inadequate and leads to erroneous results.

In general, one observation does not bring enough information to detect all 6 parameters of an elliptic orbit; this requires repeated observations and the knowledge that they refer to the same object. For this, the estimates assuming circular orbits from single observations may be helpful [3]. We do not deal with this task here. Our approach is also not applicable to objects which are not subject to Keppler's laws.

We assume that the only important forces determining the trajectory are the inertia and the Earth's gravity. This is violated when the engines of a satellite are switched on—at the time of launch or landing or during maneuvers. Deceleration due to the atmosphere is also ignored.

For LEO objects, a telescopic image gives only 2 of 4 parameters of a circular orbit. We try to get the missing parameters from fusion with Doppler radar data.

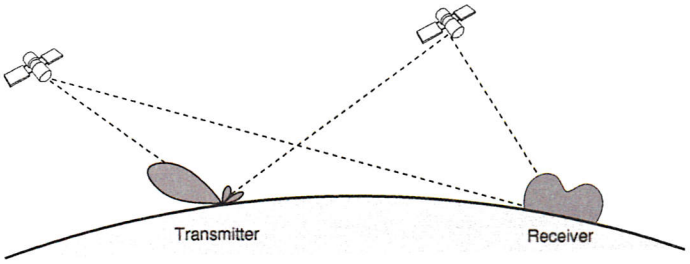

Fig. 1: Bi-static radar setup. The GRAVES transmitter radiates some power via its side lobes towards the receiver, though its main power goes in the opposite direction. We are able to receive reflections in both cases. The distance receiver–transmitter is 712 km, so there is no direct reception of the carrier.

II. Doppler radar data

A. Bi-static Doppler radar setup

We are using a passive bi-static Doppler radar setup for radio observations of LEO objects. We use the signal transmitted by a terrestrial transmitter, reflected by the satellite and received by one or more terrestrial stations distant from the transmitter, as illustrated in Figure 1.

The signal from the transmitter of the French radar-based space surveillance system GRAVES (Grand Réseau Adapte à la Veille Spatialle; Large Network Adapted to Space Watch) is passively used. The transmitter located near Dijon, France, transmits a continuous wave signal on 143.050 MHz carrier. The signal beam (main lobe) irradiates the vertical angle interval of elevations between 15° and 40°. In azimuthal direction, the beam has the radiation angle of 7.5° and sweeps a 45° wide sector in 6 steps, each for 3.2 s. Four antenna fields transmit simultaneously into four sectors, covering azimuthal range from 90° to 270°, i.e., the transmitter radiates to the south. However, it is assumed that the antenna system has some side/rear lobes that radiate to the north. We proved in our experiments that we are able to receive reflected signal from both the main and side lobes.

We use data provided to us by Czech Radio-Astronomers Amateur Network. The network consists of several amateur receivers located across the Czech Republic (the mutual distance of the receivers is about 100 km). The stations are operated either by public astronomical observatories or by private amateurs. Since the transmitter–receiver distance is 700 km or more, there is an advantage of no direct reception of GRAVES carrier. The primary aim of the network is meteors observation, when reflections of the carrier on a ionized track of a meteor upon entering the mesosphere are detected. A meteor trace causes a detectable reflection lasting several seconds, with the frequency of the carrier, possibly with small Doppler shift (10–30 Hz) caused by winds.

In contrast to meteors, reflections from (LEO) satellites can be observed up to 2 minutes and possess a characteristic pattern of Doppler shift. Since the meteor detection does not need an accurate measurement of frequency of the reflection, currently a majority of stations cannot provide precise information about the received frequency.

We are measuring the Doppler shift of the GRAVES carrier, reflected by a LEO object. Our requirements on precision of frequency measurement (5 Hz at 143.05 MHz, i.e., relative error $3.5 \cdot 10^{-8}$) pose requirements on stability and accuracy of the local oscillator of a receiver mixer. Currently only one station can provide us with suitable data (its distance to GRAVES is 712 km). Our future work includes upgrading and using the other stations.

The receiver is equipped with a ground-plane antenna type. Its sensitivity is independent of the azimuth, with a slight preference of smaller elevations, as sketched in Figure 1.

The receiver is able to detect reflections from satellites at altitudes ≤ 1000 km with RCS about $5\,\mathrm{m}^2$ or more. Thus it can be used only for LEO objects. In our experiments, satellites are detected in total distance from the receiver up to 2000 km.

B. Characterization and preprocessing of radio data

The receiver produces a quadrature signal on intermediate frequency that is digitised in 2×16 bit channels (I and Q channel) at 48 kHz sampling frequency. Thus the received frequency band around the carrier has sufficient width w.r.t. the assumed Doppler shifts of LEO objects (several kHz).

As a preprocessing, 2D spectrograms are computed from the data, using the sliding window FFT of the complex quadrature signal, with non-overlapping $1/3$ s long window. For a given time interval, the spectrogram is represented as a matrix, three rows per second, where each row contains magnitudes of FFT coefficients in the selected frequency range (typically ± 7 kHz around the carrier). The phase of FT is not used. An example of a typical spectrogram of an ISS[1] fly-over is shown in Figure 2.

A single signal from the radar at a given time gives us one real variable, enabling us to reduce the number of degrees of freedom by 1. To determine the 2 degrees of freedom missing in the telescopic observation of a LEO object, we need more. We can use:

[1] We have problems with optical observation of large space objects (ISS, Iridium), whose magnitude can be up to -8 and this could damage the camera. As an alternative, we proposed a unique solution based on telescopic detection of large satellites illuminated by the Moon instead of the Sun.

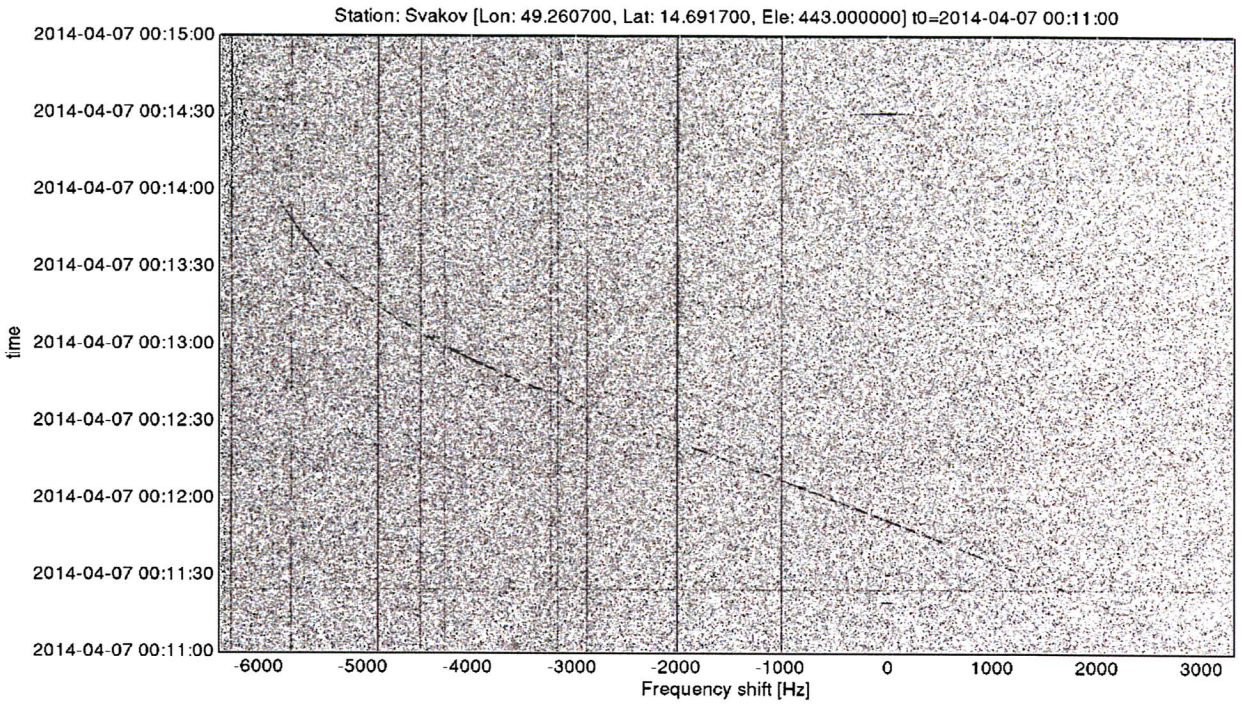

Fig. 2: Doppler shift of GRAVES carrier reflected by ISS. Magnitudes of a FFT spectra are found (more dark corresponds to more energy). The horizontal axis shows the frequency shift, where zero is for 143.050 MHz. Time flows vertically, bottom-up. Vertical lines with constant frequency are caused by local sources interferring with the high or the intermediate frequency. The dashed-line character of the Doppler shift curve is due to the switching of the transmitter beam direction which causes changes in signal intensity in one particular direction. Short events (in time) near zero shift are meteor reflections (with small Doppler shifts due to winds).

- more receivers at different positions,
- longer radar tracking.

The radar detects a longer part of the satellite fly-over, from tens of seconds to 2 minutes. This gives the frequency as a function of time. The function is represented as a sequence of points in the time-frequency domain, obtained from the detection of the curve in the spectrogram. The detection is based on specifically tailored dynamic programming techniques from computer vision, with data models suitable for radar observation incorporated. In principle, the curve of maximum energy is sought in the spectrogram. Constraints on Doppler shift at neighboring times are used to ensure curve simplicity. See example in Figure 3.

The dependence of frequency on time allows more sensitive detection and gives us much more data; the problem is with their interpretation.

C. Objects visible in radio data

For testing the processing of radio data and the detection of Doppler shift streaks, we collected data from a single receiver during two campaigns of continuous measurements:

Set 1 Feb 08 - Feb 22, 2014, 327 hours (211 GB).

Set 2 Apr 06 - Apr 28, 2014, 500 hours (322 GB).

When capturing Set 2, the receiver was equipped with a better antenna amplifier, so we have originally used Set 1 for detecting ISS only and later Set 2 has been used for observing additional satellites.

We manually annotated the data in order to analyze observability of objects and to tune/test the Doppler streak detector. We are searching for known objects–satellites selected from catalogue http://satellitedebris.net. For a particular satellite, its two-line element file (TLE) is downloaded for the observation time interval. The trajectory and speed w.r.t. the observation time is predicted. If the satellite is in direct visibility of the transmitter and the receiver, the expected Doppler shift curve is computed. Then the real spectrogram is manually examined for presence of this curve. The beginning and end times of the fly-over are manually annotated in the positive case.

We ran our Doppler streaks detector on the data. If a Doppler curve is detected, it is compared with the curve predicted from the known trajectory and it is decided whether the detection is successful or not.

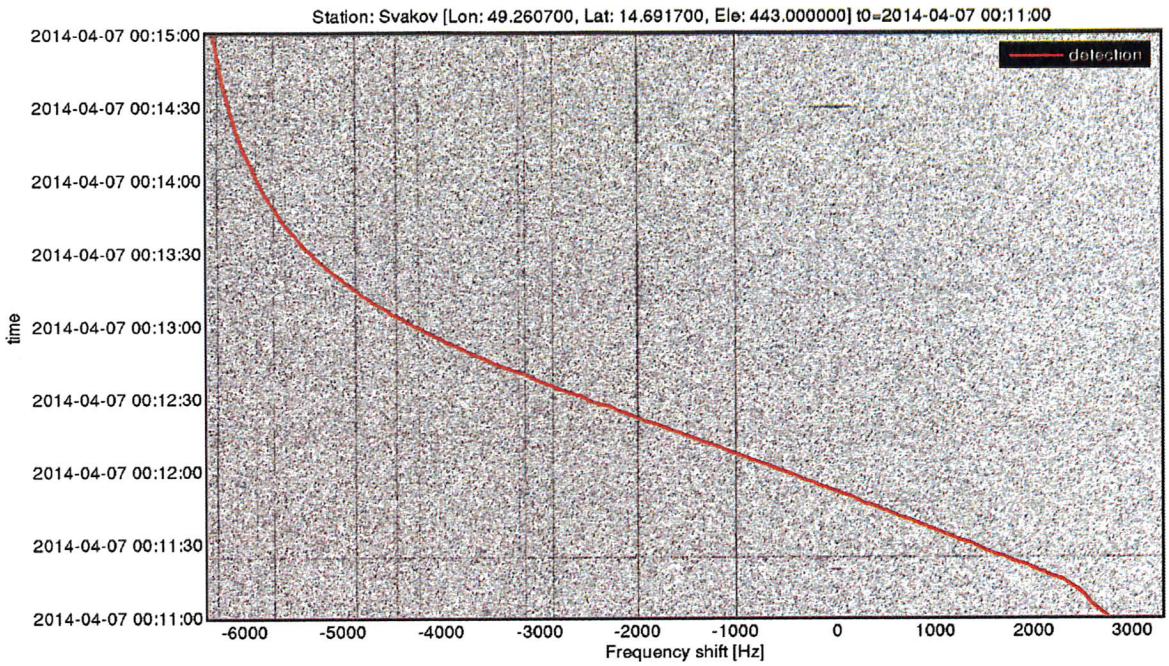

Fig. 3: Detected Doppler shift streak. The original spectrogram is shown in Figure 2.

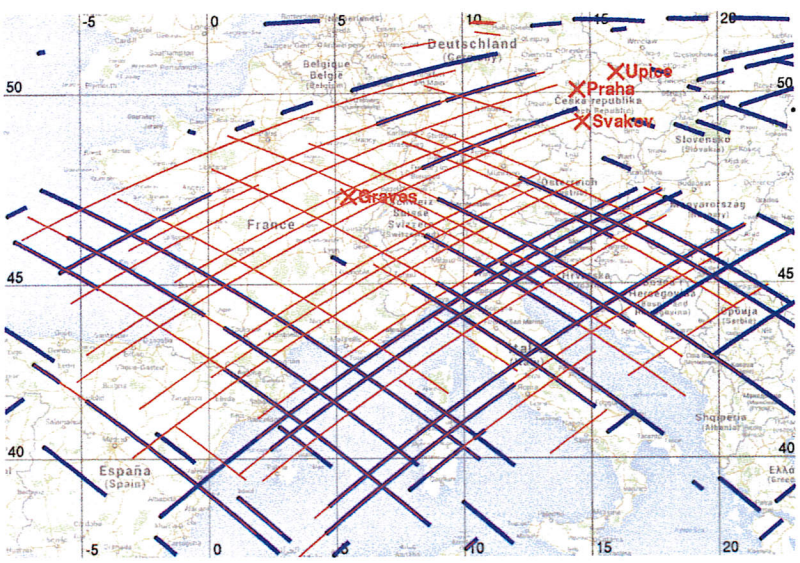

Fig. 4: Annotated and detected ISS fly-overs observed in the Set 1. Trajectory is computed from a known TLE, Doppler streak predicted and manually verified in the spectrogram. The longest fly-overs are approx. 5 minutes long. Considering the GRAVES radiating pattern, it is visible that both main and side lobes are used here. Red colour shows trajectories confirmed by annotation, blue colour emphasises trajectories that corresponds to successful detections. The blue lines that are not covered by a red line are detections that were not manually seen, yet exist in the data. Note the gap in the zenith of both the transmitter and the receiver, caused by their directional characteristics.

In Set 1, we manually annotated ISS fly-overs only, since weaker objects were not observable. There were 81 ISS fly-overs over the region, and 46 were annotated as observable. We ran our Doppler streaks detector on the data and evaluated successfully detected fly-overs. The trajectories of annotated and detected fly-overs are shown in Figure 4.

For annotation of Set 2, we selected 650 objects from the catalogue with inclination $\geq 40°$, apogee $\leq 5000\,\mathrm{km}$ and radar-cross-section (RCS) $\geq 5\,\mathrm{m}^2$. We annotated 189 hours of data (38 %), 553 fly-overs were observed. Many objects other than ISS are clearly visible, see Table I.

D. Sensitivity of radar data to permanent parameters of trajectory (orbital elements)

Analysis was done by perturbations of orbital elements of real radar observations of ISS corresponding to the following two-line element from December 29, 2013:

```
1 25544U 98067A   13363.37091435 -.00002651  00000-0 -38413-4 0  3474
2 25544 051.6485 221.2616 0005116 332.4424 005.3606 15.50013191864976
```

Object (NORAD)	Num. seen	RCS [m^2]	Apogee [km]	Perigee [km]
ISS (ZARYA) (25544)	35	396.6	417	414
TIANGONG 1 (37820)	12	20.5	375	360
ERBS (15354)	9	6.2	499	468
COSMOS 1300 (12785)	9	5.8	536	533
H-2A R/B (39580)	8	22.2	348	332
ERS 1 (21574)	8	10.9	793	746
SL-16 R/B (25861)	7	13.6	647	627
COSMOS 1340 (13067)	7	6.5	533	526
JB-3 C (28470)	7	5.4	598	548
COSMOS 2486 (39177)	6	17.7	733	711
CZ-2C R/B (39364)	6	12.8	566	476
COSMOS 1953 (19210)	6	8.7	572	554
AQUA (27424)	6	7.7	703	702
GCOM W1 (38337)	6	6.8	704	701
ADEOS (24277)	5	22.9	796	793

Table I: Annotated objects observed in Set 2. Only few of them are shown in the table, according to how many times an object was observed; there were 229 objects in 553 fly-overs in total.

The orbital elements of interest are:

- inclination $i = 51.6485°$,
- right ascencion of the ascending node $\Omega = 221.2616°$,
- semi-major axis $a = 6782.450395\,\mathrm{km}$.

Circular orbits were assumed. Each of Figures 5, 6, and 7 compares the Doppler radar responses of the real observation and two simulated fly-overs differing by inclination, right ascencion of the ascending node, and height, respectively. The black dot denotes the Graves transmitter, the red dot is the Svákov receiver, the red curves refer to the real trajectory, the blue and green ones to the perturbed trajectories. Here and in the following figures, time [s] is on the horizontal axis, the frequency shift [kHz] on the vertical one.

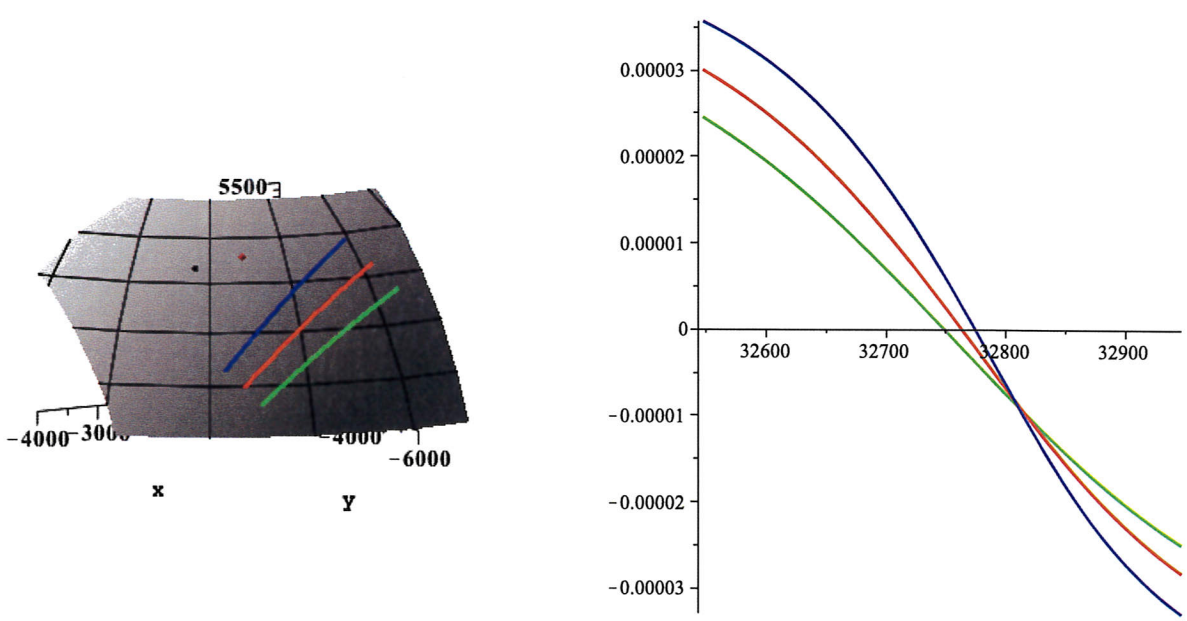

Fig. 5: Trajectories and Doppler shifts for inclinations i and $i \pm 5°$

The maximal sensitivity in the relative Doppler shift $3.5 \cdot 10^{-8}$ (5 Hz /143 MHz) represents resolution

- $\geq 3\,\mathrm{km}$ in height,
- $\geq 0.035°$ in inclination and RAAN, which is $\geq 3\,\mathrm{km}$ in position,

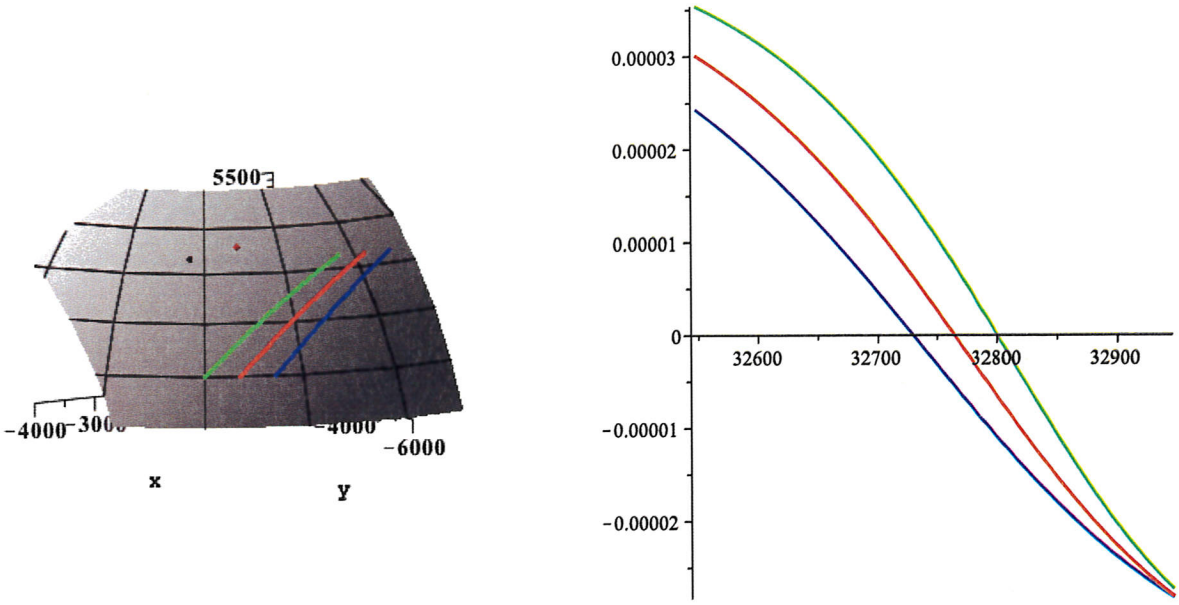

Fig. 6: Trajectories and Doppler shifts for right ascencions of the ascending node Ω and $\Omega \pm 5°$

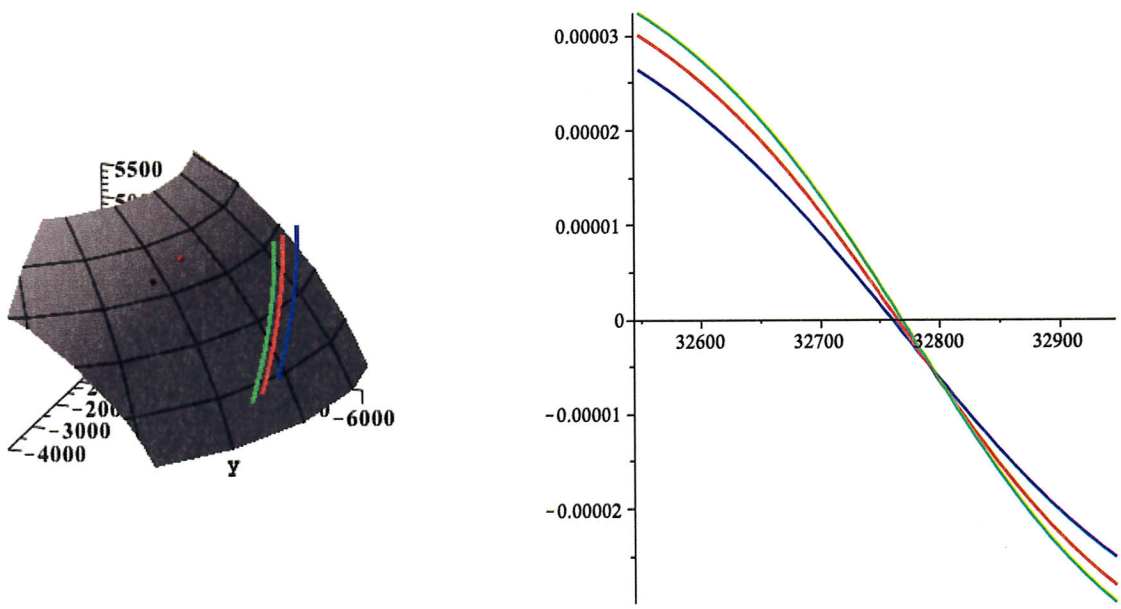

Fig. 7: Dependence on height: Trajectories and Doppler shifts for radii a, $a - 200\,\mathrm{km}$, $a + 300\,\mathrm{km}$

- $\geq 0.011°$ ($0.005°$) in mean anomaly at epoch, which is $\geq 1.5\,\mathrm{km}$ ($0.6\,\mathrm{km}$) in position at the orbit (values in brackets refer to real data from another observation).

The *best* resolution of Doppler radar is in the mean anomaly at epoch, i.e., in the orbital element which has the *worst* estimate from telescopic data.

E. Sensitivity of radar data to instantaneous parameters of trajectory

Analytical methods were applied to simulated perturbations of parameters of a real radar observation of ISS. Circular orbits were assumed. The maximal sensitivity in the relative Doppler shift $3.5 \cdot 10^{-8}$ corresponds to resolutions

- $\geq 0.07°$ in the directions satellite-transmitter and satellite-receiver ($1.5\,\mathrm{km}$ at the distance of $1000\,\mathrm{km}$),
- $\geq 0.035°$ in the direction of the velocity of the satellite ($5.5\,\mathrm{m/s}$ at the speed of $7.5\,\mathrm{km/s}$),

- $\geq 5.5\,\mathrm{m/s}$ at the speed of $7.5\,\mathrm{km/s}$ (0.07%) in the speed of the satellite (which corresponds to the difference of $10\,\mathrm{km}$ in height for circular orbits).

F. Information from Doppler radar data

The forward task—computation of the Doppler shift from a given trajectory—is easy. The inverse task—computation of a trajectory from the Doppler shifts—is hardly possible because the dependence of radar data on orbital elements is very complex. No particular features of the Doppler radar response admit a direct interpretation. E.g., the inflection point need not be unique. Nevertheless, the shape of the graph is in some sense typical for a given satellite trajectory. To fit the orbital elements to radar data, there are too many degrees of freedom. Besides, we do not have radar data from sufficiently many receivers.

A fusion of radar and telescopic data is still possible. The use of a telescopic image reduces the dimension of the search space.

III. Fusion of telescopic and radar data

The most difficult task in analysis of telescopic images is the estimation of their distance (which is related to the height). This can be estimated for circular orbits (using Kepler's Laws) provided that we know two points of the trajectory and their times. Such an input can be deduced from an image where the endpoints of a streak correspond to the beginning and end of exposure. This situation is typical for near-GEO objects, but rather rare for LEO objects. On the other hand, the radar can detect only LEO objects. The aim was to use all parameters computed from a telescopic image and estimate a single parameter—the distance—from radar data. During the work on the project we realized that there are two other unknown parameters which cannot be determined from the image:

- the time when the object passed through the FOV (for LEO objects, the endpoints of the streak are typically outside the image and the object passes about $150\,\mathrm{km}$ during the exposure time of $20\,\mathrm{s}$),
- the direction of velocity (only its sign; although most satellites rotate in the same direction as the Earth, this is not the rule and it does not have a clear meaning for polar orbits, thus we must admit also the reverse direction as a possible hypothesis).

We start from the initial set of hypotheses, which are all trajectories whose projections to the image plane lie in the line detected in the telescopic image. We compute the corresponding Doppler radar responses. Using standard optimization search techniques, we find the best-fitting hypothesis and the corresponding orbital elements. A typical result is in Figure 8.

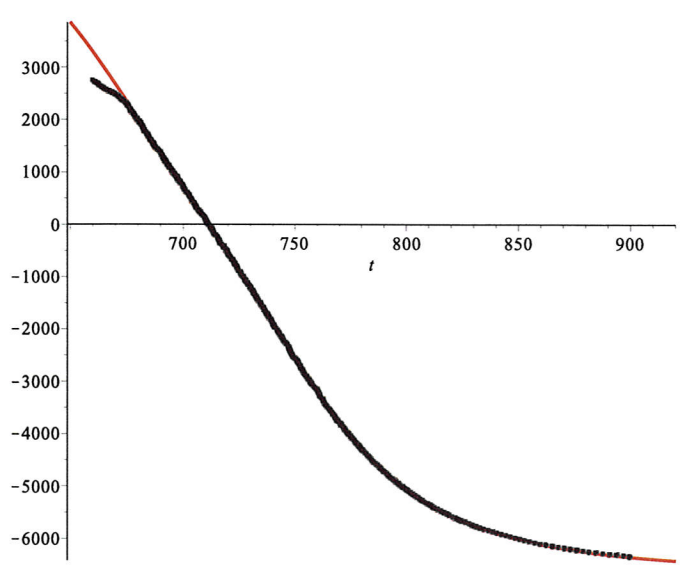

Fig. 8: Detected Doppler shifts (dark red dots) and the corresponding curve for the best-fitting model (red)

To determine the resolution of this method, we studied the dependence of the Doppler radar shift on changes of the estimated parameters, *given the corresponding streak in the telescopic image.*

This topic was analysed for simulated data and for real data from a simultaneous observation by a telescope and one Doppler radar. We used simultaneous observations of one fly-over of ISS. The telescopic image (ISS illuminated by the Moon) with exposure time $20\,\mathrm{s}$ captures $0.4\,\mathrm{s}$ of the fly-over. Radar data from receiver Svákov cover almost 2 minutes. We computed

possible circular trajectories producing the same streak in the telescopic image, depending on the unknown height, time, and sign of velocity. We fitted the model to the radar data. The best result was compared to orbital elements measured officially and included in the database of two-line elements (TLE). The nearest TLE refers to a fly-over about 3 hours later; very good agreement (better than the expected precision) has been achieved. Then we compared our best fit with models using a different height, time, or sign of velocity; the differences were evaluated.

A. Sensitivity of radar data to height *with given telescopic data (for* simulated *data)*

We used a simplified model of an object flying horizontally above a plane; the absolute values are not exact, but the sensitivity to the height is almost the same as in real situations. Figure 9 shows the sensitivity to the height (relative Doppler shift/1 km of height) for

- distance transmitter-receiver 700 km eastwards,
- height 400 km,
- several flight directions.

In all cases, the maximal resolution in height was 1 km.

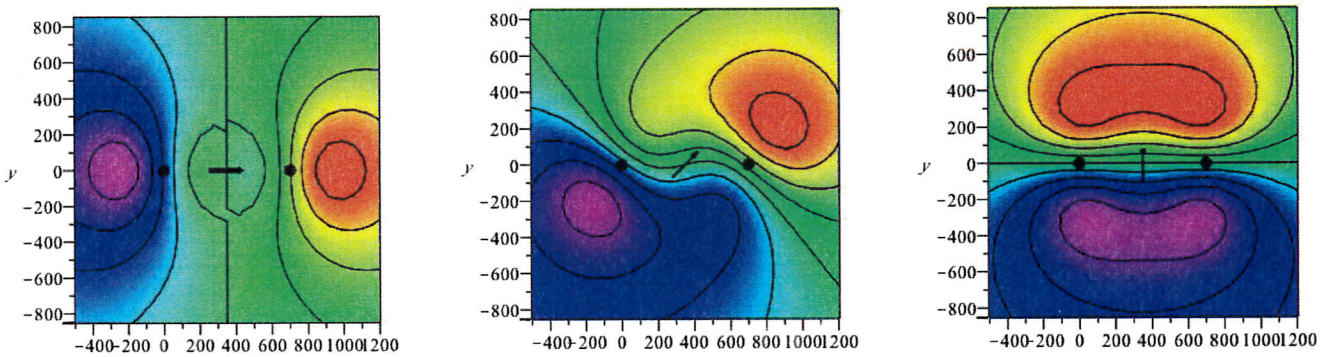

Fig. 9: Sensitivity of the Doppler shift to height as a function of horizontal position of the object [km] for various directions of velocity (arrows); small black disks denote the transmitter and the receiver

B. Sensitivity of radar data to height *with given telescopic data (for* real *data)*

A single value resulted in the resolution of up to 3 km (in simulated situations). With the whole radar observation, we achieved the resolution of up to 1 km (for real data). Data from close points carry low information, see Figure 10.

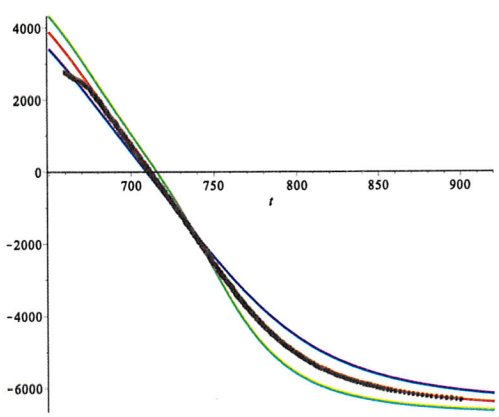

Fig. 10: Real radar detections (dark red), the best fit (red) and simulated response for height changed by ±100 km (blue and green)

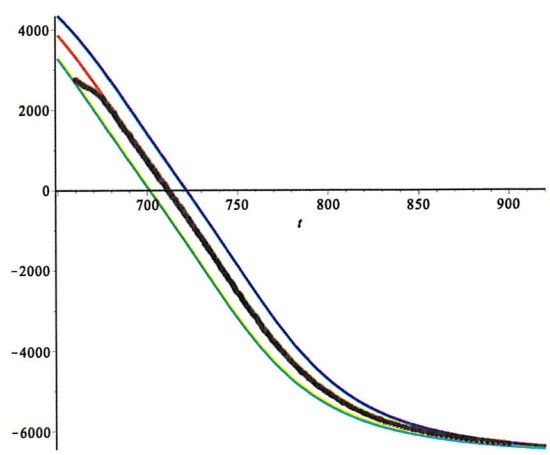

Fig. 11: Real radar detections (dark red), the best fit (red) and simulated response for time changed by ±10 s (blue and green)

C. *Sensitivity of radar data to* time *with given telescopic data (for* real *data)*

We achieved the resolution of up to 0.75 km (0.1 s, less than the window 1/3 s of the frequency analyzer!). Data from close points carry most information, see Figure 11.

D. *Sensitivity of radar data to* direction *with given telescopic data (for* real *data)*

From the telescopic image, we do not know from which side the object passed. We need to try both hypotheses and choose which of them fits better, using the fact that the responses are only approximately centrally symmetric (the influence of Earth's rotation does not change its sign). The difference is too small to be visible in the graph, but it is seen in residual errors, see Figure 12. Surprisingly, this is not trivial to decide. There are (at least theoretical) situations in which the direction cannot be decided from the data.

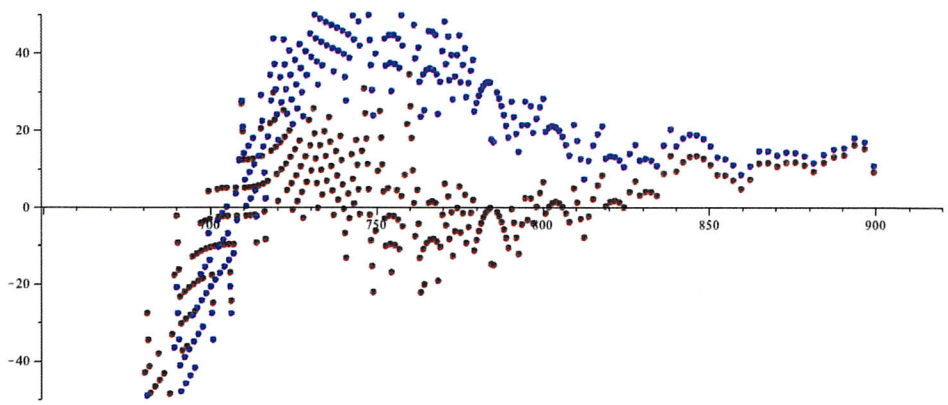

Fig. 12: Residual errors of the correct (dark red) and incorrect (blue) sign of velocity

IV. Conclusions

There is a good fit among the telescopic image, radar data, and orbital elements from the database (errors of 1 km in height, 0.02° in inclination, 0.3° in RAAN).

Data from a single radar allow us to estimate the missing parameters with a resolution better than expected (using the whole sequence of radar data instead of a single frequency). In the future, the following steps could improve the results:

- Ignoring the ends of radar detections.
- Fusion of data from more radar stations.
- Telescope at a better position (Northern Italy is the best).

V. Acknowledgement

This work was supported by the Missile Defense Agency (USA), contract 2011-0528-01 and by the Czech Science Foundation under Project P103/12/1578.

References

[1] A Collection of Satellite Database. `http://satellitedebris.net`, March 2014.

[2] A GRAVES Sourcebook. `http://www.fas.org/spp/military/program/track/graves.pdf`, Version of 2013-08-07.

[3] Yanagisawa, T., Umehara, H.: Strategy for detection of eccentric objects near the geosynchronous region. *Acta Astronautica* **65** (2009), 1001–1006.

[4] Seitzer, P. et al.: Visible Light Spectroscopy of GEO Debris. In *Proceedings of the Advanced Maui Optical and Space Surveillance Technologies Conference*, 2012.

[5] Yanagisawa, T., Kurosaki, H.: Detection of faint GEO objects using JAXAs fast analysis methods. *Transactions of the Japan Society for Aeronautical and Space Sciences*, Aerospace Technology, Japan, 10(28), 29–35, 2012.

[6] Yanagisawa, T. et al.: Comparison between four detection algorithms for GEO objects. In *Proceedings of the Advanced Maui Optical and Space Surveillance Technologies Conference*, 2012.

[7] Šára, R., Matoušek, M., Franc, V.: RANSACing Optical Image Sequences for GEO and near-GEO Objects. In *Proceedings of the Advanced Maui Optical and Space Surveillance Technologies Conference*, 2013.

[8] Navara, M., Matoušek, M.: *Sensitivity of Doppler radar to orbit parameters.* Technical report. Czech Technical University in Prague, Faculty of Electrical Engineering. Prague, 2014.

[9] Kákona, J.: *Fast multi-channel data acquisition system for radioastronomy receiver.* Master thesis. Czech Technical University in Prague, Faculty of Electrical Engineering. Prague, June 2014.

[10] Švanda, M.: *Monopole antenna for 143 MHz.* Research report. Czech Technical University in Prague, Faculty of Electrical Engineering. Prague, April 2014. In Czech.